

The main causes of changes in actual evapotranspiration and terrestrial water storage over the Eurasia inland basin

zhaofei liu¹

¹Chinese Academy of Sciences (CAS)

February 22, 2024

Abstract

The climate of the Eurasia inland basin (EIB) is characterized by limited precipitation and high potential evapotranspiration; as such, water storage in the EIB is vulnerable to global warming and human activities. There is increasing evidence pointing to varying trends in water storage across different regions; however, a consistent conclusion on the main attributes of these trends is lacking. Based on the hydrological budget in a closed inland basin, the main attributes of changes in actual evapotranspiration (AET) and terrestrial water storage (TWS) were identified for the EIB and each closed basin. In the EIB and most of its closed basins, the TWS and AET showed significantly decreasing and non-significantly increasing trends, respectively. The primary cause underpinning the significantly decreasing TWS in the EIB was increasing AET. Approximately 70% of the increase in AET has been supplied by increased irrigation diversions and glacial melt runoff. At the basin scale, similar to the EIB, changes in AET were the predominant factor driving changes in TWS in most basins; the exception to this was the Balkhash Lake basin (BLB), Iran inland river basin (IIRB), Qaidam basin (QB), and Turgay River basin (TuRB). In these basins, changes in precipitation largely contributed to the TWS changes. The AET consumption of other water resources was the main factor contributing to AET changes in seven of 16 basins, including the Aral Sea, Caspian Sea, Junggar, Monglia Plateau, Qiangtang Plateau, and Tarim River basins. The increase in precipitation contributed more than 60% of increasing AET in four of 16 basins, particularly in the Helmand River basin and QB (>90%). Changes in precipitation and consumption by other water supply sources contributed to approximately half of the AET changes in the other five basins, including the Inner Mongolia Plateau, Issyk-Kul Sarysu, BLB, IIRB, and TuRB basins.

Title: The Main Causes of Changes in Actual Evapotranspiration and Terrestrial Water Storage over the Eurasia Inland Basin

Running title: Main causes of changes in AET and TWS

Submitted to: Hydrological Processes

By

Zhaofei Liu^{1,2*}

¹ Institute of Geographic Sciences and Natural Resources Research, Chinese Academy of Sciences, 100101, Beijing, China.

² University of Chinese Academy of Sciences, 100049, Beijing, China

*Corresponding author, Zhaofei Liu (zfliu@igsrr.ac.cn)

October 6, 2021

Abstract

The climate of the Eurasia inland basin (EIB) is characterized by limited precipitation and high potential evapotranspiration; as such, water storage in the EIB is vulnerable to global warming and human activities. There is increasing evidence pointing to varying trends in water storage across different regions; however, a consistent conclusion on the main attributes of these trends is lacking. Based on the hydrological budget in a closed inland basin, the main attributes of changes in actual evapotranspiration (AET) and terrestrial water storage (TWS) were identified for the EIB and each closed basin. In the EIB and most of its closed basins, the TWS and AET showed significantly decreasing and non-significantly increasing trends, respectively. The primary cause underpinning the significantly decreasing TWS in the EIB was increasing AET. Approximately 70% of the increase in AET has been supplied by increased irrigation diversions and glacial melt runoff. At the basin scale, similar to the EIB, changes in AET were the predominant factor driving changes in TWS in most basins; the exception to this was the Balkhash Lake basin (BLB), Iran inland river basin (IIRB), Qaidam basin (QB), and Turgay River basin (TuRB). In these basins, changes in precipitation largely contributed to the TWS changes. The AET consumption of other water resources was the main factor contributing to AET changes in seven of 16 basins, including the Aral Sea, Caspian Sea, Junggar, Monglia Plateau, Qiangtang Plateau, and Tarim River basins. The increase in precipitation contributed more than 60% of increasing AET in four of 16 basins, particularly in the Helmand River basin and QB (>90%). Changes in precipitation and consumption by other water supply sources contributed to approximately half of the AET changes in the other five basins, including the Inner Mongolia Plateau, Issyk-Kul Sarysu, BLB, IIRB, and TuRB basins.

Keywords : Actual evapotranspiration; Water balance; Hydrological budget; Continental river basin; Inland closed basin; Qinghai-Tibet Plateau; Central Asia; Global Precipitation Measurement

1 INTRODUCTION

Inland basins, also referred to as endorheic basins, are defined as regions where runoff in the basin has no direct hydraulic connection with the ocean; this means that inland basin runoff is landlocked from the ocean. This runoff eventually enters inland lakes or is taken up by evapotranspiration. These regions are one of the most sensitive to climate change and human activities (Huang, Xu, Guan, Wang, & Guo, 2016; Wang et al., 2018). The Eurasia inland basin (EIB) is the largest inland basin in the world; it accounts for more than one-third of the global inland basin area and spans 20 countries. As the climate in EIBs is characterized by extremely low precipitation and high evaporation, the hydrology and ecosystem of the EIB are sensitive to changes in precipitation, actual evapotranspiration (AET), and water storage. Therefore, changes in and attribution analyses of terrestrial (or total) water storage (TWS) and AET in the EIB are hugely important to water resource management, ecosystem health and sustainable agricultural irrigation in Eurasia.

The Gravity Recovery and Climate Experiment (GRACE) is able to accurately estimate monthly TWS changes in basins that are larger than approximately 200 000 and 100 000 km² at low and high latitudes, respectively (Rodell et al., 2018). Wang et al. (2018) found that TWS was decreasing in global endorheic basins, using the GRACE TWS product; this TWS decline in the EIB contributed to 70% of the global decline. Based on three GRACE Mascon products, Rodell et al. (2018) analyzed TWS trends in 34 regions from 2002 to 2016; they categorized the drivers of this change as natural inter-annual variability, unsustainable groundwater consumption, climate change, and combinations of these factors.

In terms of basin scale research, there are inconsistent results on the main causes of water storage change, with opposing conclusions for some basins. For example, some studies have suggested that the primary cause for the water level decline in the Aral Sea was increased water consumption from enhanced human activities, particularly irrigation and damming (Yang et al., 2020). However, irrigation diversions increased from 1992 to 2005 and decreased from 2005 to 2016 (Wang et al., 2020). Thus, it was concluded that although irrigation diversion plays a dominant role in this water storage decline, its influence has been gradually weakening (Jia, Lia, Li, & Huang, 2020). Another study reported that the mountain lakes in the source region of the Aral Sea was expanding, which was mainly caused by increased glacial melt induced by elevating air temperature (Zheng et al., 2019). Several studies have shown that increasing evaporation rates play a dominant role in the water level decline in the Caspian Sea (Chen et al., 2017). Arpe, Molavi-Arabshahi and Leroy (2020) found that the decrease in net precipitation over the sea and the mean annual inflow contributed 57% and

43% to this water level decline, respectively. Other studies attributed the water level decline to increased evapotranspiration or two major earthquakes in 2000 (Elguindi & Giorgi, 2006; Ozyavas, Khan, & Casey, 2010).

In addition to the water level declines in the Aral and Caspian Seas, a decline in TWS was found to occur in other basins in the EIB, including the Iran (Joodaki, Wahr, & Swenson, 2014; Khaki et al., 2018; Moghim, 2020), Tarim (Yang, Xia, Zhan, Qiao, & Wang, 2017; Xu et al., 2019) and Turpan basins (Xu et al., 2019). The main cause for this decline in TWS in the Tarim basin is decreased precipitation (Yang et al., 2017; Xu et al., 2019). However, it was found that glacial retreat and increased water resource consumption from human activities also has an influence on TWS decline. The main factors attributed to the TWS decline in Iran differed in previous studies. Joodaki et al. (2014) found that this TWS decline was highest in the Middle East, where human activities were largely responsible for this decline. Khaki et al. (2018) found that the TWS of Iran was continuing to decrease, despite removing the influence of human activities. As such, this decline in TWS is likely to be influenced by a combination of human activities and climate change.

Increasing trends were also detected for water levels or TWS in several basins within the EIB, including water levels at Balkhash Lake (Duan et al., 2020) and Issyk-Kul Lake (Alifujiang, Abuduwaili, Ma, Samat, & Groll, 2017) and the TWS in the Qaidam (Bibi, Wang, Li, Zhang, & Chen, 2019; Meng, Su, Li, & Tong, 2019) and Qiangtang Plateau (Meng et al., 2019; Liu, Yao, & Wang, 2019) basins. Despite these research findings, there are relatively few studies that have examined the attributes of the underlying factors driving these trends.

There have also been contradictory conclusions about the TWS trends within the same region. For example, Wang et al. (2020) detected a decreasing TWS for 2002–2016 using one total water storage anomalies (TWSA) product in the Gansu Hexi Corridor basin. Cao, Nan, Cheng and Zhang (2018) found that the basin TWS significantly increased during 2002–2013 using another TWSA product. Thus, these opposing conclusions may be a result of researchers utilizing different datasets.

In summary, there continue to be inconsistent conclusions regarding changes in TWS and the main drivers of these changes in the EIB and its sub-basins. This demonstrates the need for further studies on these TWS changes and the main impact factors for these regions. The hydrologic budget (i.e., hydrologic gains and losses) is an effective method to conduct analyses at the basin scale (Liu, Yao, Huang, Wu, & Liu, 2014; Liu et al., 2016; Reager et al., 2016; Liu, Wang, & Yao, 2018). Unlike exorheic basins, which include AET and runoff in hydrologic losses, inland basins only include AET. In other words, the hydrologic budget in inland basins may only be expressed by precipitation, AET, and TWS. As such, this method is more suitable for the analysis of TWS changes and its main attribution in inland basins.

This study used multi-source data on the EIB and its closed basins to achieve three key objectives: 1) simulate the monthly AET series of each inland basin using the hydrologic budget method; 2) detect the spatiotemporal characteristics of annual and monthly precipitation, TWS, and AET using a non-parametric test method in each basin; and 3) identify the main attributions of AET and TWSA changes using the water balance principle in each closed basin.

2 MATERIALS AND METHODS

2.1 Study area

The EIB is located in the core part of Eurasia (Figure 1), spanning an area of 1.15×10^7 km²; it includes 16 closed inland basins and 23 sub-basins, which are shown in Figure 1 and Table 1. Notably, the AET simulation based on the hydrologic budget method is targeted at closed inland basins. Glaciers are distributed throughout the mountainous areas of the central and eastern basins, being mainly located in the Qinghai-Tibetan Plateau. Due to the inland location of the EIB, its climate is characterized by low precipitation and high evaporation, and the mean annual precipitation and AET are 353.4 and 358.8 mm, respectively.

The mean annual precipitation, AET, and coefficient of variation for the monthly precipitation series in each basin are shown in Table 1. There are nine closed basins in the EIB with a mean annual precipitation <200 mm; these basins are predominantly located in the eastern and southern regions. The highest mean annual precipitation occurs in the CSB, exceeding 500 mm, while lowest occurs in the TB, being <100 mm. The coefficient of variation for monthly precipitation in the EIB is 0.20; it is highest in the QPB (1.34) and lowest in the CSB (0.21).

Figure 1

Table 1

2.2 Data

2.2.1 Observed precipitation data

The observed monthly precipitation series was obtained from the Climatic Research Unit (CRU; Harris, Osborn, Jones, & Lister, 2020). There were observed 500 CRU sites within the EIB, of which the longest time series spans from 1820–2021. In this study, 139 precipitation sites spanning a data series of 1967–2020 were selected, and 123 sites with data series from 1961–2021 were used for trend analyses. Missing values were linearly interpolated based on the values in the preceding and subsequent month or the adjacent sites. The CRU gridded precipitation dataset (TS v.4.05) (Harris et al., 2020), with a $0.5^\circ \times 0.5^\circ$ resolution, was also evaluated in this study.

2.2.2 Remote sensing precipitation data

The Global Precipitation Measurement (GPM) Integrated Multi-satellite Retrievals (IMERG) Final run v.06 is a level 3 precipitation product (Huffman, Stocker, Bolvin, Nelkin, & Tan, 2019). This product using multiple precipitation-relevant satellite passive microwave sensors. The algorithm was combined with precipitation gauge analyses, microwave-calibrated infrared satellite estimates, and other precipitation estimators at a finer spatial resolution (0.1°). The data series used in this study spanned from June 2006 to December 2020.

2.2.3 GRACE TWSA data

Several versions of TWSA products have been released by several agencies; this study utilized the RL06 (v.3) GRACE liquid water equivalent thickness anomaly data series (Landerer & Swenson, 2012) from the Center for Space Research (CSR) at the University of Texas (Austin USA), the Geoforschungs Zentrum Potsdam (GFZ), and the Jet Propulsion Laboratory (JPL) in which the spatial resolution was $1^\circ \times 1^\circ$. In addition, the GRACE Mascon solutions from JPL (RL06-v2) (Watkins, Wiese, Yuan, Boening, & Landerer, 2015) and the National Aeronautics and Space Administration Goddard Space Flight Center (GSFC) (RL06-v.1) (Loomis, Luthcke, & Sabaka, 2019) were used; the spatial resolutions of these products were $0.5^\circ \times 0.5^\circ$ and $1^\circ \times 1^\circ$, respectively. These five GRACE products were abbreviated as CSR-v3, GFZ-v3, JPL-v3, JPL-v2, and GFSC-v1, and they also include the equivalent water thickness. The monthly series from April 2002 to December 2020 was used in this study. Due to the lack of observational data for validation, it was difficult to determine which product was more suitable for the EIB; as such, all five products were used to derive the TWSA trends. The spherical harmonic coefficients solution was used in three v3 products, while the mascon solution was used in the JPL-v2 and GFSC-v1 products. Post-processing filters were applied to reduce correlated errors. These solutions provide accurate surface-based gridded information, which may be well applied to studies on hydrology (Watkins et al., 2015; Save, Bettadpur, & Tapley, 2016; Loomis et al., 2019). Additional descriptions of data processing are provided in Loomis et al. (2019), Save et al. (2016), and Watkins et al. (2015).

2.3 Methods

2.3.1 Simulation of monthly AET

The hydrological budget method is an effective tool to simulate AET in inland basins. For a closed inland basin, precipitation and AET represent the hydrologic gains and losses, respectively. According to the water balance in the basin, the difference between precipitation and AET is equivalent to water storage changes in the basin; therefore, the monthly AET may be simulated as:

$$AET_i = P_i - \Delta\Sigma_i \quad (1)$$

where AET_i , P_i , and $\Delta\Sigma_i$ are the AET, precipitation, and water storage changes within a month for a closed basin, respectively, in which the unit is mm. For the gridded precipitation and TWSA data, the average data series of each closed basin was calculated based on the area weighting of each grid in the basin. For grids covered by the basin boundary, the area weighting of the boundary grid was represented by the proportion of area within the basin boundary.

In simulating the monthly AET, it is necessary to focus the consistency of the time period for each variable. Monthly precipitation and AET are the mean values within a month, computed between the beginning and end of a month. $\Delta\Sigma$ is the difference between water storage at the end and beginning of the month. However, the TWSA data used in this study represent the mean water storage within a month. Obtaining $\Delta\Sigma$ from TWSA is key to the simulation; here, $\Delta\Sigma$ was calculated as:

$$S_i = (TWSA_{i+1} - TWSA_{i-1})/2 \quad (2)$$

where $TWSA_{(i+1)}$ in the next month and $TWSA_{(i-1)}$ in the previous month represent water storage at the end of the simulated month and the beginning of the simulated month, respectively. The accuracy of this calculation has been validated by Long et al. (2014).

2.3.2 Trend detection and identification of its main attribution methods

The rank-based non-parametric Mann-Kendall (MK) test and trend magnitude method (Hirsch, Slack, & Smith, 1982) were applied to detect long-term monotonic trends and their magnitudes. This test is able to handle non-normality, censoring, data reported as “less-than” values, missing values, and seasonality; it also has high asymptotic efficiency (Fu, Charles, Liu, & Yu, 2009). Further details regarding this test were reported by Xu, Liu, Fu, & Chen (2010). The annual and monthly precipitation trends, AET, and TWSA were detected in each basin or grid.

Based on the water balance principle, the main factors causing changes in the AET and TWSA were identified. According to the water source consumed by the AET, the change in AET was attributed to changes in precipitation and the consumption of other water supply sources. Based on the hydrologic budget within a closed basin, the change in the TWSA was attributed to changes in precipitation and AET. Precipitation and AET have positive and negative effects on the TWSA; this means an increase or decrease in precipitation may prompt an increase or decrease in the TWSA, while an increase or decrease in the AET may trigger a decrease or increase in the TWSA, respectively. Similarly, precipitation and potential evapotranspiration (PET) have positive and negative effects on the AET, respectively. Based on these analyses, the main attribution of AET and TWSA changes was identified at basin scales. The contribution of precipitation and other factors to changes in the AET was semi-quantified by analyzing the magnitude of the trend between AET and precipitation.

3 RESULTS

3.1 Trends of precipitation in the EIB

Figure 2 shows trends in annual precipitation for 2002–2020 and includes gridded precipitation data from CRU and GPM and observed station data from CRU. A comparison of sites and grid data showed that the

trends in the observation sites were inconsistent with the CRU grids in some regions (Figure 2(b)). Among the 112 selected sites, trends for more than half the sites (60) were inconsistent with those of the CRU grids. For example, in the mid and downstream regions of the ASB, there was a non-significant (significance level: $p < 0.05$) increasing trend in the annual precipitation of most sites, while the corresponding CRU grids generally showed a non-significant decreasing trend. In the Mongolia and Inner Mongolia Plateau, located in the northeast EIB, there was a non-significant increasing trend in annual precipitation at most stations, while there was a decreasing trend at the corresponding CRU grids; this decreasing trend was even significant for most grids. The trends for most sites were also inconsistent with the grid results in the northern and western regions of the CSB, with some exhibiting the opposing trends in these regions.

Trends for the observed sites were highly consistent with those of the GPM grids in the EIB (Figure 2(a)). In terms of the annual precipitation trends, the majority of the CRU sites (108/112) were consistent with the GPM grids. This indicates that the GPM satellite product was highly reliable in detecting annual precipitation trends in the EIB. Therefore, the GPM precipitation data were used to analyze the precipitation trends and simulate the monthly AET series. In general, the annual precipitation was increasing in most regions, with the exception of the CSB. The significance of the increasing trend was greater at the headwater and upstream regions, and the magnitude of the trend was higher in these regions compared to the mid and downstream regions. Annual precipitation in most areas of the CSB showed a decreasing trend, particularly in the Caspian Sea and its adjacent regions. However, an opposite trend was observed in the northern region of the Volga River basin.

Figure 2

Precipitation trends in the EIB and 16 closed inland basins were detected based on the GPM satellite data. Figure 3 shows the trends in annual and monthly precipitation for each basin for 2002–2020. There was a slightly increasing trend in annual precipitation in the EIB, with the magnitude of 3.7 mm/10a. The decreasing trend was detected in the BLB, CSB, IIRB, JB, QPB and TuRB; these basins are mainly distributed in the western and northern EIB. The annual precipitation was increasing in the remaining ten basins, in which the HRB had the largest increase of 52.3 mm/10a. The magnitude of the increase in the HRB accounted for 28.6% of the mean annual precipitation in this basin. The ratio of increases to the mean annual precipitation was also relatively higher at the TB (9.9%), IMPB (7.3%), and GHCB (6.9%). The magnitude of the decrease in the IIRB also accounted for -10.8% of the mean annual precipitation in this basin. The ratio of increases or decreases to the mean annual precipitation was within $\pm 5\%$ in the remaining closed basins. The annual precipitation trends were non-significant in the EIB and each closed basin. The increasing trend in the HRB was the closest to being significant (at $p < 0.05$). However, annual precipitation showed significant decreasing trends in three sub-basins (not shown), including the Issyk-Kul Lake, Southwest Caspian Sea, and Ural River basins; the magnitudes of these decreasing trends were -86.7, -68.8, and -57.3 mm/10a, respectively.

Figure 3

3.2 Temporal variations of precipitation, AET, and TWSA in the EIB

The monthly series from the average of five GRACE TWSA products and the GPM precipitation data were used to simulate the monthly AET, utilizing the hydrologic budget method in the EIB and its 16 closed basins. The difference between precipitation and AET (described as $(P - ET)$) was also analyzed. There is a direct physical relationship between the TWS and $(P - ET)$; according to the water balance within a closed basin, the change in TWS is equivalent to the accumulated $(P - ET)$. Figure 4 presents the temporal variations in precipitation, AET, $(P - ET)$, and TWSA in the EIB. There was little difference in the mean precipitation of the EIB between months (Figure 4(b)). In terms of the intra-annual variation of precipitation at the basin scale, there were three major findings. First, there was little difference in the mean precipitation for each month in the CSB and BLB, particularly the CSB, in which the coefficient of variation was 0.24 (Table 1). This was also the major cause of the marginal difference in the monthly precipitation of the EIB,

as this precipitation accounted for a large proportion of the EIB. Second, the monthly precipitation from June to October was lower November to May of the following year in the HRB, IIRB, ASB, ISB, and TuRB. Precipitation from June to October accounted for less than 20% of the annual precipitation, in which the former two basins accounted for less than 10%. Third, under the impacts of the East Asian summer monsoon, the monthly precipitation in nine basins (i.e., GHCB, IMPB, JB, MPLB, MPIRB, QB, QPB, TaRB, and TB) in East Asia varied from month to month. The coefficient of variation exceeded 0.90. Precipitation in these basins was mainly concentrated from May to October, and this precipitation accounted for more than 80% of the annual precipitation, while it was >90% for the QB and QPB.

The mean annual precipitation and AET of the EIB for 2002–2020 was 353.4 and 358.7 mm, respectively. This indicates that water consumed by the AET was greater than the precipitation that occurred in the EIB. The number of years where $P < AET$ and $P > AET$ was similar, although the mean ($P - ET$) of the former (21.4 mm) was greater than the latter (10.1 mm). During November to March of the following year, precipitation in the EIB was able to meet the AET demand (i.e., $P > AET$); however, monthly precipitation was less than the AET from April to October. In other words, precipitation in the EIB was insufficient to meet the demand from the AET during this period.

The annual and monthly TWSA of the EIB was generally decreasing over the 2002–2020 period, particularly for 2005–2015 (Figures 8(c) and 8(d)). Overall, the results were consistent among the five TWSA products for the annual and monthly series. The accumulated ($P - ET$) was highly correlated with the TWSA series; the R^2 between the monthly series of accumulated ($P - ET$) and the mean of the five TWSA products was 0.97, and reached up to 1.00 between the two annual series. According to the standardized monthly series, the TWSA was lagging by approximately one month compared with the ($P - ET$).

Figure 4

3.3 The main attribution of AET changes in the EIB

Figure 5 presents the annual and monthly AET trends over the 2002–2020 period in the EIB and its 16 closed basins. There was a non-significant increasing trend in the annual AET of the EIB for 2002–2020, with a magnitude of 12.4 mm/10a; this was higher than the corresponding precipitation increase. By contrast, there were non-significant decreasing trends in annual AET for the BLB, IIRB, QPB, and TuRB, alongside the annual precipitation for these basins; the greatest rate of decrease occurred in the IIRB, reaching -9.7 mm/10a, which was consistent with the precipitation trends in this basin. In the remaining 12 basins, the AET was increasing, and this increase was significant in the HRB. The highest rate of increase was 56.2 mm/10a in the HRB; this is also consistent with the precipitation trends in these basins. These results indicate that precipitation is one of the important factors impacting changes in the AET. In addition, the increase in AET in the IMPB reached 34.6 mm/10a. The AET increase in the ASB, CSB, GHCB, ISB, MPLB, MPIRB, and TB was between 10 and 20 mm/10a, while this increase other basins was <10 mm/10a. Although the AET trends were consistent with those of precipitation in most basins, they showed opposite trends in the CSB and JB. In these two basins, AET and precipitation was increasing and decreasing, respectively, indicating that in addition to precipitation, the consumption of other water sources by AET is also an important factor affecting changes in AET.

Based on the main attribution identification method described in the Section 2.3.2, the main factors affecting changes in AET changes were analyzed. Additionally, the contribution of precipitation and other water sources to changes in the AET was also semi-quantified by comparing the trend magnitude of AET and precipitation. The increase in precipitation in the EIB accounted for 30% of the AET, indicating that the increasing consumption of other water sources was the dominant factor increasing the AET in the EIB. This increase in consumption may be due to a range of mechanisms: (1) increased evaporation rates from rising temperature; and (2) increased irrigation diversion and glacial melt runoff, producing an increase in AET.

At the basin scale, the increase in precipitation accounted for more than 60% of the increase in AET in the HRB, QB, GHCB, and TB, particularly the two former basins, where this proportion exceeded 90%. This

indicates that the main factor affecting the increase in AET in these basins was higher precipitation.

In the ASB, TaRB, MPLB, and MPIRB, the proportion of precipitation increase that contributed to the AET increase was <30%, and the proportion was <10% for the former two basins. This indicates that the higher precipitation only made a relatively small contribution to the AET increase. The increase in the consumption of other water sources caused by enhanced evaporation rates played a dominant role in the increasing AET. In the CSB and JB, precipitation was decreasing, potentially inducing a decrease in the AET as there are reduced water sources for evaporation consumption; however, the AET in these basins was increasing, indicating that increased evaporation rates consumed other AET water sources. This is the main reason underpinning the increasing AET in these two basins. In the QPB, the AET decrease only accounted for 4% of the decrease in precipitation. This means that as precipitation decreased by -9.6 mm/10a, the increasing ET consumption of other water sources from enhanced evaporation was the main contributor to the restricted AET of only -0.4 mm /10a in the basin.

In the BLB, IIRB, and TuRB, the decrease in AET accounted for $50\% \pm 2\%$ of the decrease in precipitation; this means enhanced evaporation rates led to the consumption of other water sources, resulting in an increasing AET. This partially compensated for the AET decrease in the basins, and indicates that the increases consumption of other water sources and the precipitation decrease accounted for approximately half of the AET decrease. In the IMPB and ISB, the precipitation increase accounted for $50\% \pm 4\%$ of the AET increase, indicating that the increase in precipitation and the consumption of other water resources as a result of enhanced evaporation rates contributed to approximately half of the change in the AET.

Figure 5

3.4 The main attribution of TWS changes in the EIB

Figure 6 shows the spatial distribution of the TWSA trends in the EIB for 2002–2020; generally, this distribution was similar among the five products, in which significant decreasing trends were observed in most regions. The highest decreasing magnitude was observed in the Caspian Sea region. The TWSA showed that there were significant increasing trends in several regions, including headwater regions (mainly located in the Qinghai-Tibetan Plateau) of the QB, QPB, and TaRB in the southeastern EIB and a small part of the north-central EIB (headwaters of the northwest BLB). In addition, the TWSA also showed non-significant increasing trends in some headwater regions of the Volga River. Although the spatial distribution of trends was consistent among the five products, there were clear differences in the magnitude of the trends for the Caspian Sea region, especially at the core part of the Caspian Sea. The decreasing magnitude of two mascon products exceeded -70 cm/10a at the core part of the Caspian Sea, which is more than twice that of the v3 products.

Figure 6

TWSA trends in the EIB and its 16 closed basins were analyzed using the average series from the five GRACE products. Figure 7 presents the annual and monthly TWSA trends for different basins for 2002–2020. As opposed to the large variation in precipitation trends each month, there was only a slight variation in the TWSA trends between each month. The standard deviation of the magnitude of TWSA trends ranged between 0.3 and 0.9 among the different closed basins, while it was 0.4 for the entire EIB. This is because the seasonal variation of soil moisture, glacier/snow, surface and ground waters in TWS is much lower than precipitation. The lowest seasonal variation occurred in the QPB, as there are a large number of solid water bodies (glacial and snow covered) in this region, and these water bodies were relatively stable in terms of TWS. There were significant decreasing trends in the annual and monthly TWSA in the EIB, exceeding a significance level of $p < 0.01$.

At the closed basin scale, although the annual TWSA was decreasing in most basins, there were slight and significant increasing trends in the QPB and QB, with the magnitude of 0.2 and 5.7 cm/10a, respectively. The increasing annual and monthly TWSA in the QB exceeded the significance level of $p < 0.001$. The annual

and monthly TWSA in the BLB showed non-significant decreasing trends. There were significant decreasing trends in annual TWSA in the remaining 12 basins. With the exception of the MPLB and MPIRB, the significance levels in the other ten basins exceeded $p < 0.01$. The decreasing magnitude was highest in the IIRB and CSB, at -9.2 and -8.9 cm/10a, respectively.

Figure 7

Across the entire EIB, it was expected that the increase in precipitation would cause an increase in the TWSA; however, the TWSA showed a significant decreasing trend. This indicates that the increase in water consumption by the AET was the main factor driving the significant decrease in the TWSA. Figure 8 shows the trends in the annual precipitation, AET and TWSA, mean annual precipitation and AET, and the accumulated ($P - ET$) values in each closed basin. In general, precipitation, AET, and changes in TWSA were in balance at the closed basin scale; however, the changes in P, AET and TWSA were not in balance. As such, the contribution from changes in precipitation and AET to changes in TWSA at the closed basin scale was qualitatively analyzed.

Similar to the EIB, there were significant decreasing trends in the TWSA when precipitation exhibited increasing trends in most basins, including the ASB, GHCB, HRB, IMPB, ISB, MPLB, MPIRB, TaRB, and TB. This indicates that the increase in AET was the main cause of the significant decrease in the TWSA in these basins. In the CSB and JB, the decrease in precipitation and the increase in AET led to a decrease in the TWSA. The increasing magnitude of AET was three and 1.5 times the decreasing magnitude of precipitation in the CSB and JB, respectively. This indicates that the increase in AET contributed to the decrease in the TWSA to a greater extent than did the decrease in precipitation. The results for the BLB, IIRB, and TuRB were the opposite to those of the aforementioned basins. It was expected that the decreasing AET would induce an increase in the TWSA; however, the TWSA exhibited significant or non-significant decreasing trends in these basins. This indicates that the decrease in precipitation was the main factor affecting the decrease in the TWSA of these basins. The decreasing precipitation in the QPB may cause a decrease in the TWSA; however, there was a slightly increasing trend in the TWSA of the basin, largely due to the decrease in the AET. The increasing in the AET for the QB may cause a decrease in TWSA; however, there was a significant increasing TWSA in the basin largely caused by the increasing precipitation.

According to the physical influence mechanism, the change in the TWSA in a closed basin is directly correlated to the accumulated ($P - ET$), and this study was able to verify this. For the depth results, the accumulated ($P - ET$) for 2002–2020 was -5.3 cm/10a; this is consistent with the decreasing magnitude of TWSA in the EIB. At the basin scale, the magnitude of trends of TWSA in each basin ranged from -9.2 to 5.7 cm/10a, with an average of -3.0 cm/10a. The accumulated ($P - ET$) in each basin varied from -9.6 to 6.2 cm/10a, with a mean of -3.1 cm/10a. There was a high consistency between the TWSA changes and accumulated ($P - ET$). The results were similar to the depth results for the EIB and each basin. The TWSA decreased by $-5615.6 \times 10^8 \text{ m}^3/10\text{a}$ during 2002–2020 in the EIB. This annual reduction in the TWSA in the EIB was approximately equivalent to the mean annual runoff of the Yellow River. At the basin scale, the decreasing magnitude of the TWSA was relatively higher in the western and southwestern basins of the EIB, including the CSB, IIRB, ASB, and HRB; the magnitude of the decrease in the CSB exceeded than $-3300 \times 10^8 \text{ m}^3/10\text{a}$. The amount of accumulated ($P - ET$) was consistent changes in the TWSA; the R^2 between the two series composed from each basin value reached 0.99.

Figure 8

4 DISCUSSION

4.1 Literature comparison of the main attribution results

The main attribution of changes in AET and TWSA in the EIB were semi-quantified based on the water balance in the closed basin. The main contribution to the decrease in the TWSA was the increase in the AET. The incremental AET consumption of other water sources and the precipitation increase contributed

approximately 70% and 30% to the increased AET, respectively. Although few studies have focused on the entire EIB, there have been many studies focusing on the attribution to changes in TWSA at the basin scale; these results were compared with the results from this study. For example, the Caspian Sea level has been gradually decreasing over the past 20 y. Some studies have attributed this decrease to meteorological factors (van Dijk, Renzullo, Wada, & Tregoning, 2014), while others suggest that evaporation from the sea is the main impact factor (Chen, et al., 2017). Other studies have suggested that it is these two factors combined with agricultural irrigation diversions (Rodell et al., 2018). According to the water balance of the closed basins, this study demonstrates that the main factor causing the decreasing sea level was the increase in AET. The increase mainly includes an increase in water surface evaporation and agricultural irrigation diversion. For example, the Volga River delivers roughly 80% of its runoff to the Caspian Sea; however, there are 11 dams located in the basin that ensures a steady water supply for crop irrigation (Avakyan, 1998; Rodell et al., 2018). There was a negligible correlation between crop production and precipitation, suggesting that irrigation effectively mitigates the impact of drought. Based on the long-term observation data from 1961 to 2020, there was a clear dry period over the past 20 y (Figure 6). Therefore, the runoff into the Caspian Sea has decreased due to the inevitable increase in agricultural irrigation diversion throughout this dry period. In addition, the reservoir capacity of dams in the CSB exceeds 75% of the total inflow, and the total capacity of reservoirs is 223 km³; these dams mostly occur in the Volga River basin (Akbari et al., 2020). Although precipitation in the headwaters of the Volga River is increasing, the impact of increased precipitation on runoff into the sea may be weakened as a result of water storage regulation of reservoirs during the dry seasons. Therefore, the precipitation increase in the headwaters has a limited impact on the Caspian Sea level.

The extent to which the increase in AET has contributed to the TWSA decline in the ASB from 2002 to 2020 was greater than the decreasing precipitation; this is consistent with the conclusions of previous studies (Yang et al., 2020). The increase in the AET consumption of other water sources contributed >90% to the increase in AET, while the precipitation increase contributed <10%. The increase in AET consumption of other water sources largely involves the increase in water surface evaporation caused by higher evaporation rates and the increase in AET from irrigation diversion. Although the impact of agricultural irrigation diversion on the water storage of the basin has been gradually weakening post-2005 (Wang et al., 2020), agricultural irrigation diversion remains the most important water resource problem in this region. There is still a need to improve the irrigation efficiency, crop use efficiency, and water resource management in this region. The precipitation decrease was the main impact factor driving the decrease of the TWSA in the IIRB; this is consistent with previous studies (Khaki et al., 2018).

The significant increasing trend in the TWSA for the QB and QPB was consistent with previous studies (Bibi et al., 2019; Meng et al., 2019; Liu et al., 2019); however, the main causes attributed to this trend differ from those identified in previous studies. The increasing TWSA in the QB is mainly caused by the precipitation increase, which contributes >90 % to the increase in AET. In the QPB, the increasing TWSA has largely been attributed to the decrease in AET.

Similar to the ASB results, the increase in AET was also the main cause for the decrease in the TWSA for the TaRB; this differs from the results of previous studies (Yang et al., 2017; Xu et al., 2019). The extent to which the increase in AET consumption of other water sources contributed to the increasing AET (>90%) was much higher than that of precipitation (<10%). The increase in the AET consumption of other water sources was mainly due to the elevated consumption of water resources by human activities and the increase in melt water from glacier retreat.

There were non-significant decreasing trends in the TWSA of the BLB and ISB for 2002–2020; this is contrary to the rising water levels in Balkhash Lake and Issyk-Kul Lake reported in previous studies (Alifujiang et al., 2017; Duan et al., 2020) and may be due to the differences in the study period. These two study periods for the previous works ended in 2012 and 2013, respectively, while this study period ended in 2020. The precipitation decrease and the increase in the AET consumption of other water sources from elevated evaporation rates accounted for approximately half of the AET changes in the BLB and ISB.

Based on the results of five GRACE TWSA products, there was a significant decreasing trend in the TWSA for the GHC for 2002–2020. This differed from the results obtained at other time periods when only one product was used (Cao et al., 2018; Wang et al., 2020). Similar to the EIB and most of its closed basins, the decreasing TWSA of the GHC was mainly due to the increase in AET; >60% of the precipitation increase contributed to the AET increase.

4.2 GRACE TWSA products and uncertainties

It was difficult to determine which product was more suitable for the EIB because of the lack of observational data for validation. However, the area of the Caspian Sea is sufficiently large and thus, may be considered a typical region to evaluate TWSA products. Chen et al. (2017) found that the observed level of the Caspian Sea decreased by -67.2 cm/10a for 1996–2015. This was more consistent with the two mascon products (JPL-v2 and GFSC-v1), compared to the three spherical harmonic coefficients products (CSR-v3, GFZ-v3, and JPL-v3). This was because the TWSA of the Caspian Sea from the two mascon products decreased by >-60 cm/10a for 2002–2020, as consistent with the observed decrease. The TWSA of the three other products was <-33 cm/10a, which is much lower than the observed value; this indicates that the mascon products in the Caspian Sea region outperforms the spherical harmonic coefficients products. Some studies have also highlighted the many advantages of the mascon products for hydrologic studies (Scanlon et al., 2016; Rodell et al., 2018). Overall, the five TWSA products showed high consistency in most other regions of the EIB.

The uncertainties associated with the AET simulation were mainly due to uncertainties in the input data and during simulation processes. As the input precipitation and TWSA data were grid data, the actual basin boundary did not coincide with the grid boundary. In this study, the area weighting of the basin in the boundary grids was used to reduce the uncertainty caused by the lack of alignment with the two boundaries. Many studies have shown that GPM precipitation products have high accuracy at regional scales (Tang, Ma, Long, Zhong, & Hong, 2016; Le, Lakshmi, Bolten, & Bui, 2020; Islam, Yu, & Cartwright, 2020); this was also the case in this study, in which the GPM precipitation products were highly consistent with the station observations in the EIB. Although the five TWSA products were generally highly consistent in the EIB, there were still some differences (e.g., Figures 8(c) and 8(d)). This study used the mean value series of five TWSA products to simulate the monthly AET series, causing uncertainties in the simulated AET. In addition, we also compared the median value series of the five products, finding marginal differences between the mean and median series. Monthly AET series simulated by the two series were also highly consistent. The accuracy of GRACE TWSA data directly determined the accuracy of the related applications. As such, further research on GRACE TWSA inversion is required for hydrology and water resource applications.

In the simulation of monthly AET, ΔS represents the change in the water storage over a month (i.e., the difference between the water storage at the end and beginning of the month). However, the GRACE TWSA data represents the mean water storage in the month. In this study, the difference between the TWSA of the previous month and the next month was used to represent the ΔS in the basin; this may also have caused uncertainties. This study simulated the monthly AET series for a closed basin, in which the runoff process within the basin was ignored; however, for a finer temporal scale or an exorheic basin, the runoff process within the basin must be considered.

5 CONCLUSIONS

A method of monthly AET simulation using public satellite precipitation and TWS data was proposed utilizing the hydrologic budget within a closed inland basin. As these data are available at a global scale, the method may easily be applied to simulate monthly AET in other closed inland basins. In addition, trends in annual and monthly precipitation, TWS, and AET were detected using the MK test. The main attributions of AET and TWSA changes were identified for the EIB and each of its closed basins.

There was a slightly increasing trend in the annual precipitation of the EIB for 2002–2020, with a magnitude of 3.7 mm /10a. A decreasing trend was detected in the western and northern basins, including the BLB, CSB, IIRB, JB, QPB, and TuRB. The highest increasing and decreasing magnitude was 52.3 and -20.4 mm/10a

in the HRB and IIRB, accounting for 28.6% and 10.8% of the mean annual precipitation, respectively; all these trends were non-significant. In the EIB and most of its closed basins, the TWSA and AET showed significant decreasing and non-significant increasing trends, respectively. The increasing trends of the TWSA were mainly detected at the Qinghai-Tibetan Plateau, including the QB (significant) and QPB, and some headwater regions.

The increasing AET water consumption was the dominant factor affecting the significant decrease in TWSA in the EIB. The consumption of other water sources, mainly included irrigation diversion and glacial melt runoff, accounted for 70% of the increasing AET. At the basin scale, changes in the AET were the main factor impacting changes in the TWSA in most basins, including the ASB, CSB, GHCB, HRB, IMPB, ISB, JB, MPLB, MPIRB, QPB, TaRB, and TB. Changes in precipitation played a dominant role in changes for the TWSA in the BLB, IIRB, QB, and TuRB. Similar to the EIB, the consumption of other water resources was the main factor driving the changes in the AET for the ASB, CSB, JB, MPLB, MPIRB, QPB, and TaRB. However, the precipitation increase contributed >60% to the elevated AET in the HRB, QB, GHCB, and TB, particularly in the former two basins, where the contribution exceeded 90%. Changes in precipitation and the consumption of other water sources contributed approximately half of the AET changes in the IMPB, ISB, BLB, IIRB, and TuRB.

ACKNOWLEDGEMENTS

This study was supported and funded by the Strategic Priority Research Program of the Chinese Academy of Sciences (XDA2006020202; XDA23090302) and the National Natural Science Foundation of China (4217011346; 41661144030). We would like to thank X. Zhang for the data processing.

REFERENCES

- Akbari, M., Baubekova, A., Roozbahani, A., Gafurov, A., Shiklomanov, A., Rasouli, K., . . . Haghghi, A.T. (2020). Vulnerability of the Caspian Sea shoreline to changes in hydrology and climate. *Environmental Research Letters* , 15 , 115002.
- Alifujiang, Y., Abuduwaili, J., Ma, L., Samat, A., & Groll, M. (2017). System dynamics modeling of water level variations of Lake Issyk-Kul, Kyrgyzstan. *Water* , 9 , 989.
- Arpe, K., Molavi-Arabshahi, M., & Leroy, S.A.G. (2020). Wind variability over the Caspian Sea, its impact on Caspian seawater level and link with ENSO. *International Journal of Climatology* , 40 , 6039–6054.
- Avakyan, A.B. (1998). Volga-Kama cascade reservoirs and their optimal use. *Lakes & Reservoirs: Research and Management* , 3 , 113–121.
- Bibi, S., Wang, L., Li, X., Zhang, X., & Chen, D. (2019). Response of groundwater storage and recharge in the Qaidam Basin (Tibetan Plateau) to climate variations from 2002 to 2016. *Journal of Geophysical Research: Atmospheres* , 124 , 9918–9934.
- Cao, Y., Nan, Z., Cheng, G., & Zhang, L. (2018). Hydrological Variability in the Arid Region of Northwest China from 2002 to 2013. *Advances in Meteorology* , 2018 , 1502472.
- Chen, J.L., Pekker, T., Wilson, C.R., Tapley, B.D., Kostianoy, A.G., Cretaux J.F., & Safarov, E.S. (2017). Long-term Caspian Sea level change. *Geophysical Research Letters* , 44 , 6993–7001.
- Duan, W., Zou, S., Chen, Y., Nover, D., Fang, G., & Wang, Y. (2020). Sustainable water management for cross-border resources: The Balkhash Lake Basin of Central Asia, 1931-2015. *Journal of Cleaner Production* , 263 , 121614.
- Elguindi, N., & Giorgi, F. (2006). Projected changes in the Caspian Sea level for the 21st century based on the latest AOGCM simulations. *Geophysical Research Letters* , 33 , 4–7.
- Fu, G.B., Charles, S.P., Liu C.M., & Yu, J.J. (2009). Decadal climatic variability, trends and future scenarios for the North China Plain. *Journal of Climate* , 22 , 2111–2123.

- Harris, I., Osborn, T.J., Jones, P., & Lister, D. (2020). Version 4 of the CRU TS monthly high-resolution gridded multivariate climate dataset. *Scientific Data* , 7 , 109.
- Hirsch, R.M., Slack, J.R., & Smith, R.A. (1982). Techniques of trend analysis for monthly water quality data. *Water Resources Research* , 18 , 107–121.
- Huang, J., Xu, H., Guan, X., Wang, G., & Guo, R. (2016). Accelerated dryland expansion under climate change. *Nature Climate Change* , 6 , 166–171.
- Huffman, G.J., Stocker, E.F., Bolvin, D.T., Nelkin, E.J., & Tan, J. (2019). GPM IMERG Final Precipitation L3 1 month 0.1 degree x 0.1 degree V06, Greenbelt, MD, Goddard Earth Sciences Data and Information Services Center (GES DISC). <https://doi.org/10.5067/GPM/IMERG/3B-MONTH/06>. (Accessed September 2, 2021)
- Islam, A., Yu, B.F., & Cartwright, N. (2020). Assessment and comparison of five satellite precipitation products in Australia. *Journal of Hydrology* , 590 , 125474.
- Jia, Q.M., Lia, Y.P., Li, Y.F., & Huang, G.H. (2020). Analyzing variation of inflow from the Syr Darya to the Aral Sea: A Bayesian-neural-network-based factorial analysis method. *Journal of Hydrology* , 587 , 124976.
- Joodaki, G., Wahr, J., & Swenson, S. (2014). Estimating the human contribution to groundwater depletion in the Middle East, from GRACE data, land surface models, and well observations. *Water Resources Research* , 50 , 2679–2692.
- Khaki, M., Forootan, E., Kuhn, M., Awange, J., van Dijk, A.I.J.M., Schumacher, M., & Sharifi, M.A. (2018). Determining water storage depletion within Iran by assimilating GRACE data into the W3RA hydrological model. *Advances in Water Resources* , 114 , 1–18.
- Landerer, F.W., & Swenson, S. C. (2012). Accuracy of scaled GRACE terrestrial water storage estimates. *Water Resources Research* , 48 , W04531.
- Le, M.H., Lakshmi, V., Bolten, J., & Bui, D.D. (2020). Adequacy of Satellite-derived Precipitation Estimate for Hydrological Modeling in Vietnam Basins. *Journal of Hydrology* , 586 , 124820.
- Liu, W. B., Wang, L., Zhou, J., Li, Y. Z., Sun, F. B., Fu, G. B., ... Sang, Y. F. (2016). A worldwide evaluation of basin-scale evapotranspiration estimates against the water balance method. *Journal of Hydrology* , 538 , 82–95.
- Liu, Z., Wang, R., & Yao, Z. (2018). Climate change and its impact on water availability of large international rivers over the mainland Southeast Asia. *Hydrological Processes* , 32 , 3966–3977.
- Liu, Z., Yao, Z., Huang, H., Wu, S., & Liu, G. (2014). Land use and climate changes and their impacts on runoff in the Yarlung Zangbo River basin, China. *Land Degradation and Development* , 25 , 203–215.
- Liu, Z., Yao, Z., & Wang, R. (2019). Automatic identification of the lake area at Qinghai–Tibetan Plateau using remote sensing images. *Quaternary International* , 503 , 136–145.
- Long, D., Longuevergne, L., & Scanlon, B.R. (2014). Uncertainty in evapotranspiration from land surface modeling, remote sensing, and GRACE satellites. *Water Resources Research* , 50 , 1131–1151.
- Loomis, B.D., Luthcke, S.B. & Sabaka, T.J. (2019). Regularization and error characterization of GRACE mascons. *Journal of Geodesy* , 93 , 1381–1398.
- Meng, F., Su, F., Li, Y., & Tong, K. (2019). Changes in terrestrial water storage during 2003–2014 and possible causes in Tibetan Plateau. *Journal of Geophysical Research: Atmospheres* , 124 , 2909–2931.
- Moghim, S. (2020). Assessment of Water Storage Changes Using GRACE and GLDAS. *Water Resources Management* , 34 , 685–697.

- Ozyavas, A., Khan, S.D., & Casey, J.F. (2010). A possible connection of Caspian Sea level fluctuations with meteorological factors and seismicity. *Earth and Planetary Science Letters* , 299 , 150–8.
- Reager, J.T., Gardner, A.S., Famiglietti, J.S., Wiese, D.N., Eicker, A., & Lo, M.H. (2016). A decade of sea level rise slowed by climate-driven hydrology. *Science* , 351 , 699-703.
- Rodell, M., Famiglietti, J.S., Wiese, D.N., Reager, J.T., Beaulieu, H.K., Landerer, F.W., & Lo, M.H. (2018). Emerging trends in global freshwater availability. *Nature* , 557 , 651–659.
- Save, H., Bettadpur, S., & Tapley, B.D. (2016). High resolution CSR GRACE RL05 mascons. *Journal of Geophysical Research: Solid Earth* , 121 , 7547–7569.
- Scanlon, B.R., Zhang, Z., Save, H., Wiese, D.N., Landerer, F.W., Long, D., ... Chen, J. (2016). Global evaluation of new GRACE mascon products for hydrological applications. *Water Resources Research* , 52 , 9412–9429,
- Tang, G.Q., Ma, Y.Z., Long, D., Zhong, L.Z., & Hong, Y. (2016). Evaluation of GPM Day-1 IMERG and TMPA Version-7 legacy products over Mainland China at multiple spatiotemporal scales. *Journal of Hydrology* , 533 , 152–167.
- van Dijk, A.I.J.M., Renzullo, L.J., Wada, Y., & Tregoning, P. (2014). A global water cycle reanalysis (2003–2012) merging satellite gravimetry and altimetry observations with a hydrological multi-model ensemble. *Hydrology and Earth System Sciences* , 18 , 2955–2973.
- Wang, J.D., Song, C.Q., Reager, J.T., Yao, F.F., Famiglietti, J.S., Sheng, Y.W., ... Wada, Y. (2018). Recent global decline in endorheic basin water storages. *Nature Geoscience* , 11 , 926–932.
- Wang, S., Liu, H., Yu, Y., Zhao, W., Yang, Q., & Liu, J. (2020). Evaluation of groundwater sustainability in the arid Hexi Corridor of Northwestern China, using GRACE, GLDAS and measured groundwater data products. *Science of the Total Environment* , 705 , 135829.
- Wang, X., Chen, Y., Li, Z., Fang, G., Wang, F., & Liu, H. (2020). The impact of climate change and human activities on the Aral Sea Basin over the past 50 years. *Atmospheric Research* , 245 , 105125.
- Watkins, M.M., Wiese, D.N., Yuan, D.N., Boening, C., & Landerer, F.W. (2015). Improved methods for observing Earth's time variable mass distribution with GRACE. *Journal of Geophysical Research: Solid Earth* , 120 , 2648–2671.
- Xu, M., Wang, X., Sun, T., Wu, H., Li, X., & Kang, S. (2019). Water balance change and its implications to vegetation in the Tarim River T Basin, Central Asia. *Quaternary International* , 523 , 25–36.
- Xu, Z.X., Liu, Z.F., Fu, G.B., & Chen, Y.N. (2010). Hydro-climate trends of the Tarim River Basin for the last 50 Years. *Journal of Arid Environments* , 74 , 256–267.
- Yang, P., Xia, J., Zhan, C., Qiao, Y., & Wang, Y. (2017). Monitoring the spatio-temporal changes of terrestrial water storage using GRACE data in the Tarim River basin between 2002 and 2015. *Science of the Total Environment* , 595 , 218–228.
- Yang, X., Wang, N., Chen, A., He, J., Hua, T., & Qie, Y. (2020). Changes in area and water volume of the Aral Sea in the arid Central Asia over the period of 1960–2018 and their causes. *CATENA* , 191 , 104566.
- Zheng, G., Bao, A., Li, J., Zhang, G., Xie, H., Guo, H., ... Chen, W. (2019). Sustained growth of high mountain lakes in the headwaters of the Syr Darya River, Central Asia. *Global and Planetary Change* , 176 , 84–99.

Table 1 Abbreviations, mean annual precipitation and AET for each inland closed basin in the EIB

ID	Sub basins	Closed basins	Abbreviations	Annual Precipitation (mm)
1	Amu Darya River	Aral Sea basin	ASB	326.4

ID	Sub basins	Closed basins	Abbreviations	Annual Precipitation (mm)
2	Syr Darya River			
3	Balkhash Lake basin	Balkhash Lake basin	BLB	381.5
4	Eastern Caspian Sea	Caspian Sea basin	CSB	578.1
5	Caspian Sea			
6	Ural River basin			
7	Volga River basin			
8	Southwest Caspian Sea			
9	Chu-Talas Rivers	Issyk-Kul Sarysu basin	ISB	365.6
10	Issyk-Kul Lake basin			
11	Sarysu River			
12	Gansu Hexi Corridor basin	Gansu Hexi Corridor basin	GHCB	153.3
13	Helmand River basin	Helmand River basin	HRB	182.8
14	Inner Mongolia Plateau basin	Inner Mongolia Plateau basin	IMPB	216.8
15	Iran inland river basin	Iran inland river basin	IIRB	188.1
16	Junggar basin	Junggar basin	JB	189.7
17	Monglia Plateau lake basin	Monglia Plateau lake basin	MPLB	181.6
18	Monglia Plateau inland river basin	Monglia Plateau inland river basin	MPIRB	151.3
19	Qaidam basin	Qaidam basin	QB	147.8
20	Qiangtang Plateau basin	Qiangtang Plateau basin	QPB	264.8
21	Tarim River basin	Tarim River basin	TaRB	112.9
22	Turgay River basin	Turgay River basin	TuRB	316.7
23	Turpan basin	Turpan basin	TB	86.2

Figure Caption

Figure 1 Location and distribution of each basin in the EIB (number represents each basin as shown in Table 1).

Figure 2 Annual precipitation trends for 2002–2020 detected at (a) GPM; and (b) CRU grids and CRU observation sites.

Figure 3 Annual and monthly precipitation trends for EIB and its 16 closed basins for the 2002–2020 period.

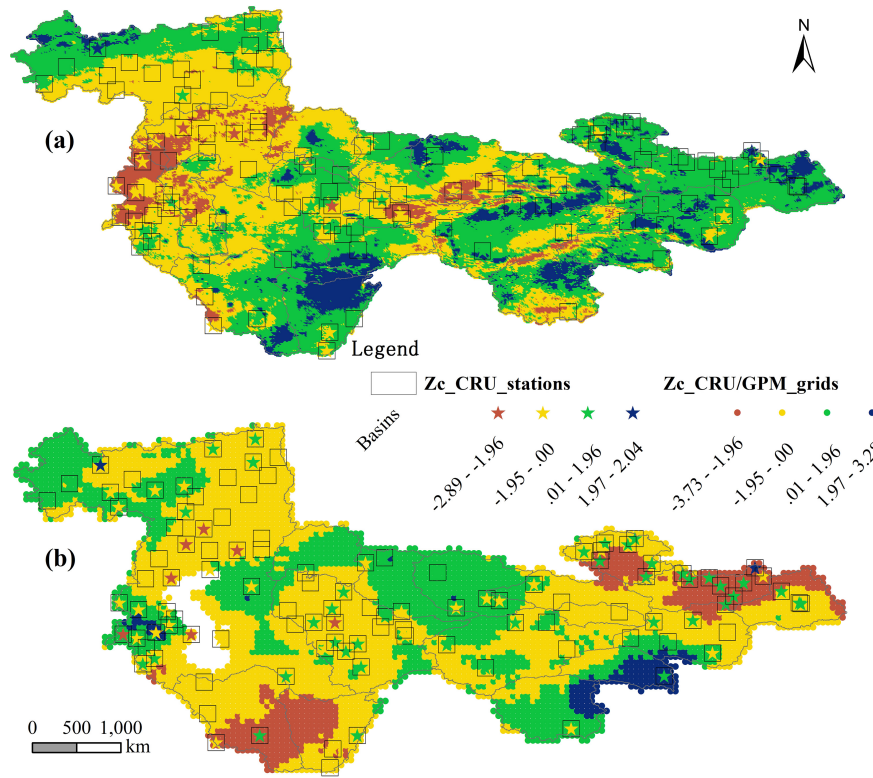
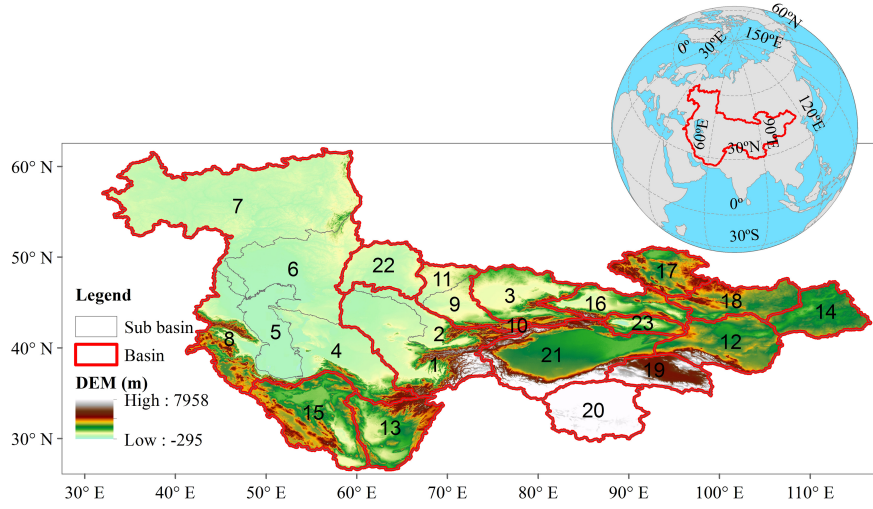
Figure 4 Temporal variations in precipitation, AET, ($P - ET$), and TWS in the EIB: (a) and (b) precipitation, AET, and ($P - ET$) at the intra-annual and inter-annual scales, respectively; (c) annual series of the TWSA range from five GRACE products and accumulated ($P - ET$); (d) similar to (c) using a monthly series.

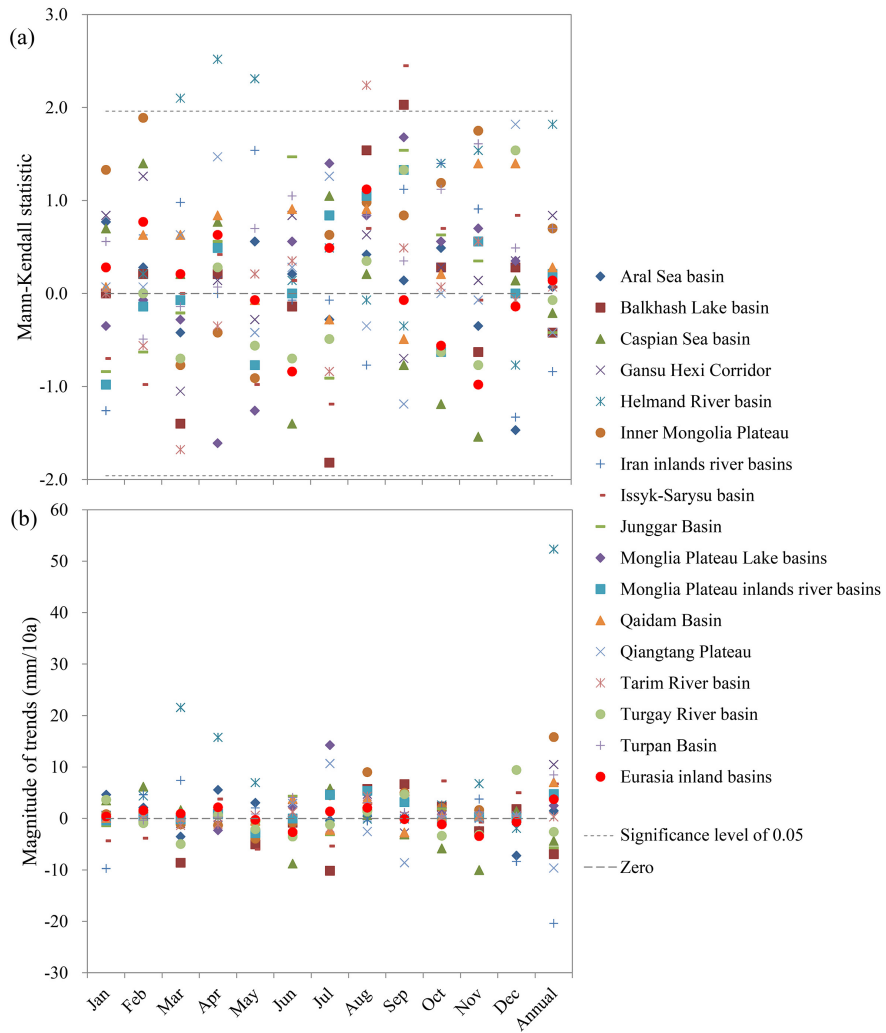
Figure 5 Annual and monthly trends of ET for EIB and its 16 closed basins during the 2002–2020 period.

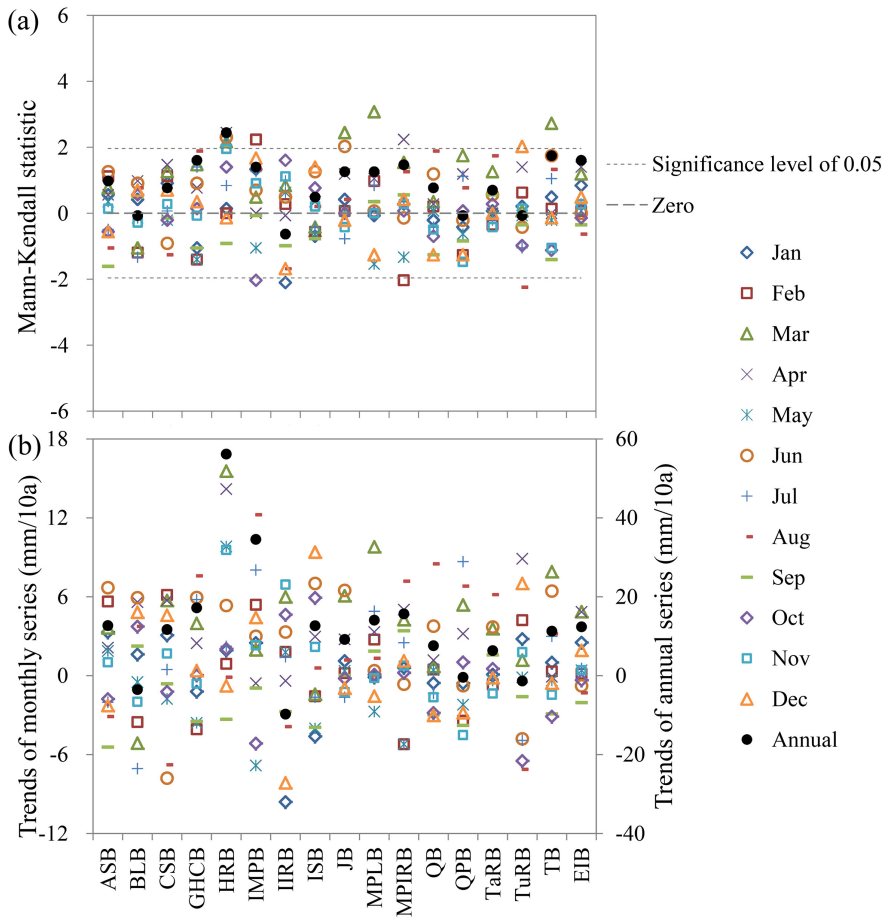
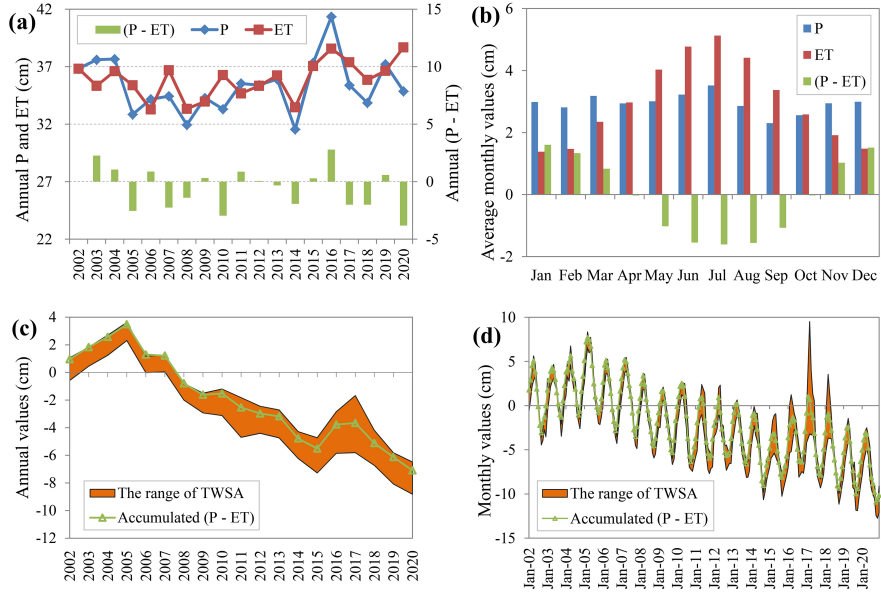
Figure 6 Spatial distribution of TWSA trends in the EIB for 2002–2020: (a) to (e) represent the CSR-v3, GFZ-v3, JPL-v3, JPL-v2 and GFSC-v1, respectively.

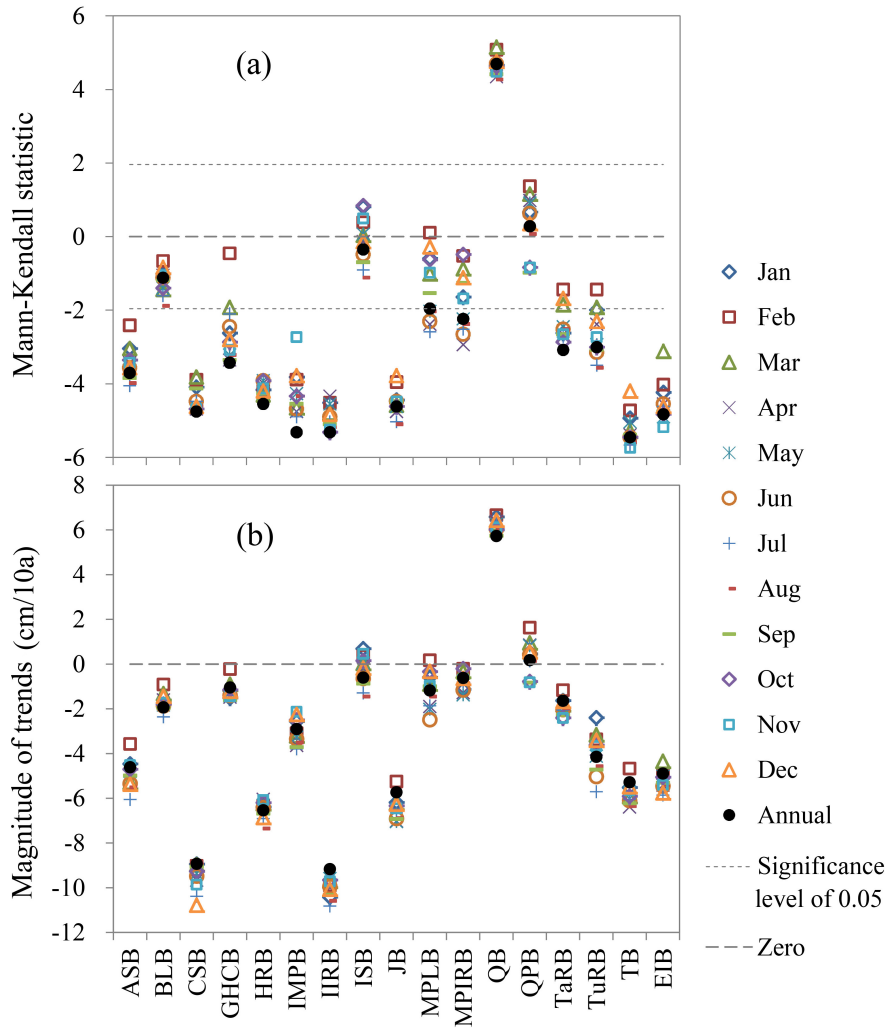
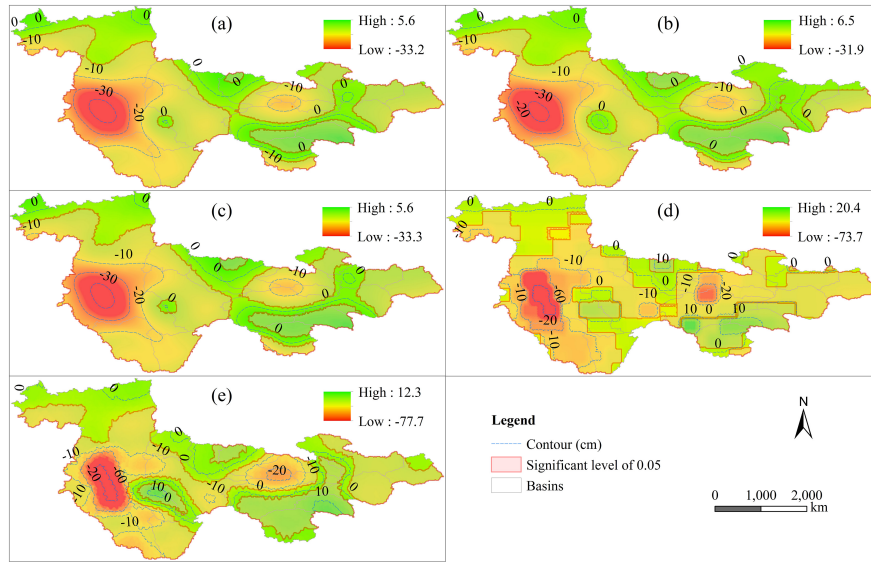
Figure 7 Annual and monthly trends of TWSA for EIB and its 16 closed basins during the 2002–2020 period.

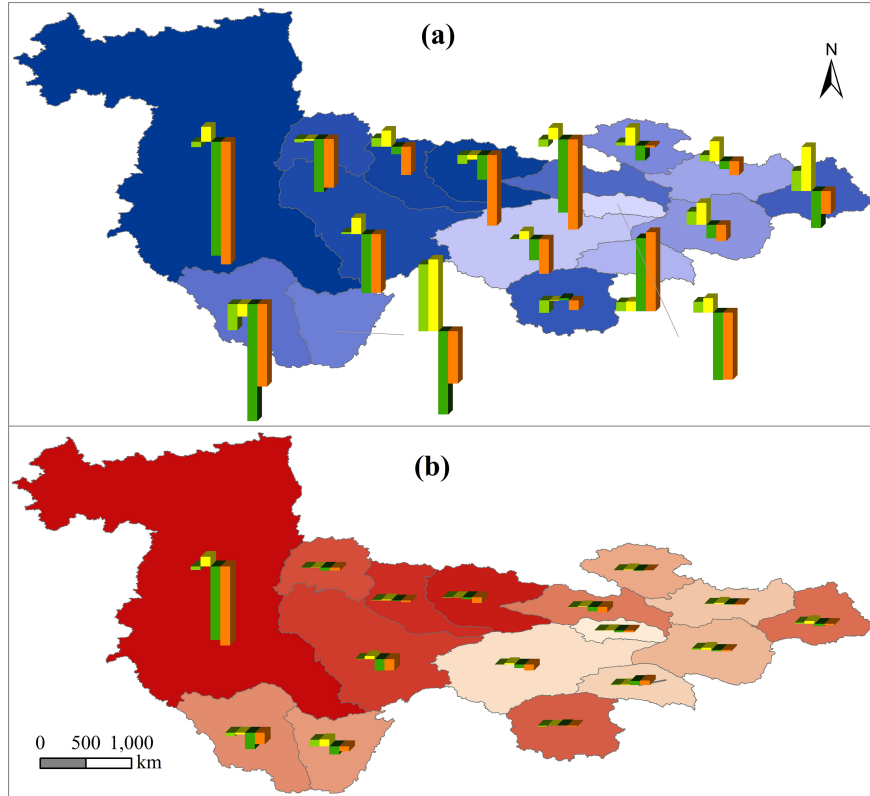
Figure 8 Trends in annual precipitation (P), evapotranspiration (ET) and TWSA, and mean annual P , ET , and accumulated ($P - ET$) values in each basin: (a) and (b) are the depth and amount units, respectively.









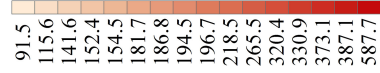


Legend

Mean annual precipitation (mm)



Mean annual evapotranspiration (mm)



Depth (cm/10a)



Amount (10⁸ m³/10a)



- P
- ET
- TWSA
- Accumulated (P-ET)